








RESEARCH ARTICLE | APRIL 10 2024

## Remote inductively coupled plasmas in Ar/N<sub>2</sub> mixtures and implications for plasma enhanced ALD

Special Collection: [Atomic Layer Deposition \(ALD\)](#)

David R. Boris ; Michael J. Johnson ; Jeffrey M. Woodward ; Virginia D. Wheeler ; Scott G. Walton 

 Check for updates

*J. Vac. Sci. Technol. A* 42, 033008 (2024)

<https://doi.org/10.1116/6.0003538>



# Remote inductively coupled plasmas in Ar/N<sub>2</sub> mixtures and implications for plasma enhanced ALD

Cite as: J. Vac. Sci. Technol. A 42, 033008 (2024); doi: 10.1116/6.0003538

Submitted: 13 February 2024 · Accepted: 20 March 2024 ·

Published Online: 10 April 2024



David R. Boris,<sup>1,a)</sup>  Michael J. Johnson,<sup>1</sup>  Jeffrey M. Woodward,<sup>2</sup>  Virginia D. Wheeler,<sup>2</sup>   
and Scott G. Walton<sup>1</sup> 

## AFFILIATIONS

<sup>1</sup>U.S. Naval Research Laboratory, Plasma Physics Division, 4555 Overlook Ave. SW, Washington, DC 20375

<sup>2</sup>U.S. Naval Research Laboratory, Electronics Science and Technology Division, 4555 Overlook Ave. SW, Washington, DC 20375

**Note:** This paper is part of the 2024 Special Topic Collection on Atomic Layer Deposition (ALD).

**a) Electronic mail:** [david.boris@nrl.navy.mil](mailto:david.boris@nrl.navy.mil)

## ABSTRACT

Plasma enhanced atomic layer deposition (PEALD) is a cyclic atomic layer deposition (ALD) process that incorporates plasma-generated species into one of the cycle substeps. The addition of plasma is advantageous as it generally provides unique reactants and a substantially reduced growth temperature compared to thermal approaches. However, the inclusion of plasma, coupled with the increasing variety of plasma sources used in PEALD, can make these systems challenging to understand and control. This work focuses on the use of plasma diagnostics to examine the plasma characteristics of a remote inductively coupled plasma (ICP) source, a type of plasma source that is commonly used for PEALD. Ultraviolet to near-infrared spectroscopy and spatially resolved Langmuir probe measurements are employed to characterize a remote ICP system using nitrogen-based gas chemistries typical for III-nitride growth processes. Spectroscopy is used to characterize the relative concentrations of important reactive and energetic neutral species generated in the remote ICP as a function of gas flow rate, Ar/N<sub>2</sub> flow fraction, and gas pressure. In addition, the plasma potential and plasma density for the same process parameters are examined using an RF compensated Langmuir probe downstream from the ICP source. The results are also discussed in terms of their impact on materials growth.

<https://doi.org/10.1116/6.0003538>

## I. INTRODUCTION

Over the last two decades, plasma enhanced atomic layer deposition has played an increasingly important role in the advanced manufacturing and semiconductor sectors, in large part because the technique enables low temperature growth of thin films with atomic scale precision on a wide variety of substrates.<sup>1–3</sup> While there are significant advantages to the plasma-based approach for atomic layer deposition (ALD), the use of plasma also comes with substantial complexity.<sup>3</sup>

While a variety of plasma sources can be used for plasma enhanced atomic layer deposition (PEALD), the remote inductively coupled plasma (ICP) is one of the most common types of sources due to its ability to effectively dissociate and excite the gas used in the reactant step, while spatially separating the production of ions

from the growth substrate. At high reactor pressures, this allows one to deliver reactive neutral species to the surface while limiting the flux of ions to the surface, a potential source of film damage. Alternatively, the pressure can be reduced, and ions can be used as a means to drive the surface out of thermal equilibrium with the bulk substrate, encouraging the growth of crystalline films at low temperature.<sup>3</sup>

A significant body of work has been dedicated to understanding the operation of inductively coupled plasma sources.<sup>4–13</sup> Less has been done examining the details of remote ICPs used in PEALD configurations,<sup>14–18</sup> where the ICP source is powered by a helical antenna encompassing a dielectric tube with a diameter much smaller than that of the downstream growth reactor. This type of geometry has been shown to display nonlocal electron

25 April 2024 03:49:28

kinetics (in which the electron energy relaxation length exceeds the device dimensions),<sup>16,19</sup> particularly under low pressure conditions, which affect the plasma density, electron energy distribution function (EEDF), and plasma potential. These effects will have consequences for the energy flux density delivered by the ions to substrate surfaces. As such, understanding and managing the operation of such systems is critically important, particularly when remote ICPs are operated with the intent of growing crystalline films.<sup>3,17,18,20,21</sup>

The manner in which electromagnetic fields generated by the RF antenna heat the EEDF is an important aspect governing how remote ICP sources function. Generally, ICP sources couple power from the antenna into the plasma via two electron heating modes: the electrostatic mode (E-mode) and the electromagnetic mode (H-mode). The E-mode is characterized by capacitive coupling between the electric field generated by the antenna inductance and the plasma electrons, and the H-mode is characterized by inductive coupling between the antenna and plasma electrons. ICP sources operating in a steady state condition will generally adopt one of these two modes. In the case of H-mode operation, there will usually be a transition from the E-mode to the H-mode during the start-up phase of the discharge.<sup>13</sup> The H-mode is broadly characterized by a higher power transfer efficiency to the plasma and higher plasma density, which should result in a higher density of reactive neutrals and ions within the plasma source volume. The significant difference between these two modes of operation makes it of interest to characterize remote ICP sources in terms of how different operating conditions influence electron heating modes and their influence on downstream reactive neutral and charged particle characteristics near the growth substrate.

This work focuses on the evolution of plasma conditions in nitrogen-based chemistries as this gas mixture is commonly used in the reactant step of nitride PEALD recipes.<sup>22–25</sup> The effect of ICP source geometry is also examined by employing two different commercial ICP sources with different orifice diameters and antenna diameters. The sources examined in this work are the Fiji G1 and Fiji G2 remote ICP sources manufactured by Veeco. The details of these systems are provided in Sec. II A. Generally, the conditions examined in this work will be confined to those obtainable in commercial PEALD systems. As such, the measurements will focus on pressure ranges between about 1 and 300 mTorr. Reactors fitted with turbo-molecular pumps are able to reach low pressure regimes ( $\sim$ few mTorr), where crystalline film growth has been observed using PEALD protocols.<sup>21,26</sup> In contrast, reactors without turbo-molecular pumps are typically limited to higher pressure regimes ( $>150$  mTorr). Operating pressures between these two regimes would require the use of a conductance limited valve or other pumping speed throttles.

We combine optical emission spectroscopy (OES) and Langmuir probe measurements to determine how the plasma characteristics respond to changes in critical operating parameters such as neutral pressure, total gas flow, and relative gas flows of Ar and N<sub>2</sub>. OES is utilized to characterize the relative concentrations of atomic N generated in ICP systems. Plasma density,  $n_e$ , electron temperature,  $T_e$ , and plasma potential,  $V_p$ , for the same process parameters are examined using an RF compensated Langmuir probe. Changes in species densities and the associated flux of either

reactive and/or energetic species have been established as key drivers of the PEALD growth process.<sup>17,27</sup> Therefore, the plasma density and plasma potential are of particular interest in that they are the key parameters in determining the flux and energy of charged species at the growth surface.

## II. EXPERIMENT

The custom-built plasma diagnostics reactor, shown in Fig. 1, consists of an 8 in. Conflat 6 way cross, pumped by a 250 l/s Varian turbo-pump. The base pressure in this system is  $\approx 5 \times 10^{-7}$  Torr. A conductance-limiting valve is used to adjust the pressure and allowed plasma generation in pressure regimes ranging from  $\sim 1$  mTorr to  $\sim 1$  Torr. The multiple ports on this reactor enable diagnostic access (visual and physical) to a volume extending from the orifice of the ICP source to about 25 cm downstream, a range that corresponds reasonably well to the source-to-substrate distance in typical growth tools utilizing the remote ICP sources. The diagnostics available on this reactor include UV-NIR spectroscopy as well as spatially resolved Langmuir probe measurements.

### A. Plasma sources

In this work, we examined two plasma sources: the Veeco Fiji G1 and Fiji G2 remote ICP sources, designated as G1 and G2, respectively. Notable differences between the sources include source length, dielectric tube diameter, antenna geometry, and the orifice diameter at the chamber end. Both are powered by a Seren R301 RF amplifier, which is connected through a Seren AT Series matching network in an L-type network topology. The antenna geometries differ between the systems: the G1 source antenna has 8 turns over approximately 13 cm, while the G2's spans 10 turns over about 17 cm. Importantly, in the G1 case, the ground termination for the antenna is near the orifice of the source leading into the reactor, conversely, in the G2 case the ground termination of the antenna is far from the reactor orifice near the gas inlet. The diameter of the antenna coils also differs significantly along with the diameters of the dielectric tubes around which the antennas are wrapped. The G1 coil encompasses a quartz tube with an inner diameter of 1.6 cm (0.625 in.) and an outer diameter of 1.9 cm (0.75 in.), while the G2 coil surrounds a quartz tube with an inner diameter of 3.49 cm (1.38 in.) and an outer diameter of 3.81 cm (1.5 in.). This leads to significantly different plasma generation volumes with the G2 source volume being approximately six times larger than the G1. Accordingly, the power deposition per unit volume differs for a given operating power.

### B. Optical emission spectroscopy

Visible to near-infrared (Vis-NIR) spectral measurements in the range of 630–830 nm were taken using an Ocean Optics HR2000+ spectrometer. The spectrometer, equipped with a 1200 g/mm grating, offers a 0.1 nm spectral resolution and allows for rapid measurements with broadband spectral information. In Fig. 1(b), the survey spectrum is acquired using plasma conditions of 300 W RF power, 40 mTorr neutral pressure in a 10% Ar, 90% N<sub>2</sub> gas mixture with a total flow of 44 SCCM. The figure shows the

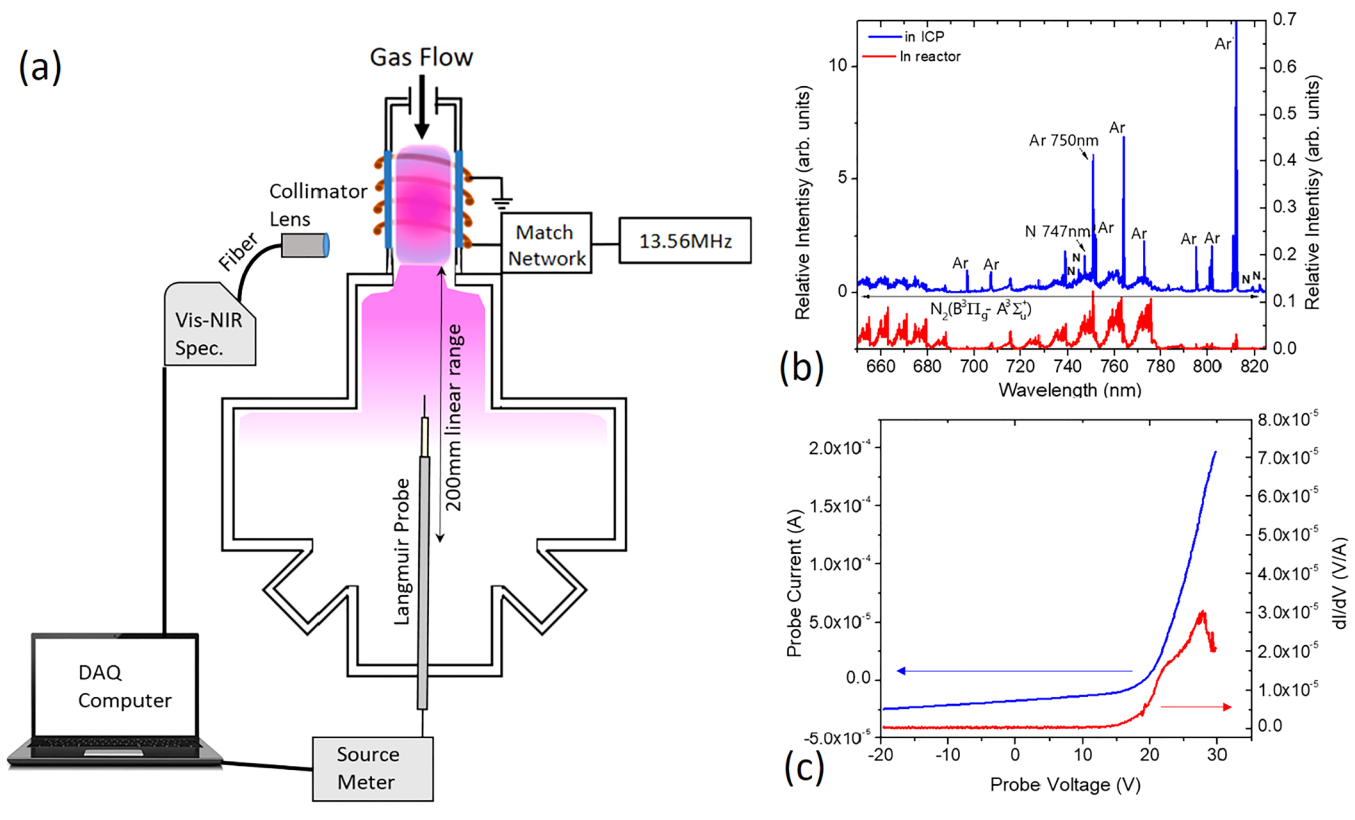


**FIG. 1.** (a) Plasma diagnostics reactor (drawing not to scale) showing the available diagnostics suite including UV-NIR spectroscopy and a movable, RF compensated Langmuir probe. (b) A survey spectrum using the Visible-NIR spectrometer with prominent atomic Ar and atomic N lines denoted. Note the spectral range includes the first positive system of electronically excited N<sub>2</sub>. Conditions are 30 mTorr with 40 SCCM N<sub>2</sub> and 4 SCCM Ar flow at 300 W RF power. (c) An exemplary Langmuir probe trace was taken at 20 cm from the orifice of the Fiji G1 plasma source using the same operating conditions. All Langmuir probe measurements were performed on the centerline of the chamber.

25 April 2024 03:49:28

relevant N(I) line at 747 nm used for measuring the concentration of atomic N relative to the Ar concentration.<sup>28</sup> The Ar 750 nm line is also highlighted along with a number of prominent vibrational bands in the first positive system of N<sub>2</sub> (B<sup>3</sup>Π<sub>g</sub> – A<sup>3</sup>Σ<sub>u</sub><sup>+</sup>). These data and all others monitoring atomic line emission for the purpose of obtaining atomic N densities were performed perpendicular to the axis of the ICP near the exit orifice, as shown in Fig. 1(a).

The spectral response of the spectrometer was determined using an OL-550 (Optronic Laboratories, Inc.) calibrated tungsten halogen light source, and the spectra were corrected to account for the obtained transmission function. Applying the transmission function to the OES data allows for the use of the line ratio method to obtain an absolute measure of atomic N densities. N atom density was monitored as a function of N<sub>2</sub>/(N<sub>2</sub> + Ar) flow fraction, total pressure in the reactor, and total flow in the reactor.

### C. Line ratio method

OES provides both a qualitative and quantitative description of species present in a plasma. Species are identified via their emission at a given wavelength, generated when a given species

undergoes a high-to-low energy electron state transition. Comparing the emission line intensity of a specific line against the line intensity of a species with a known density allows one to determine the density of that species. As such, a ratio of emission lines was used to determine the concentration of N within the plasma. The line ratio technique was used to measure the ratio of excited atomic N\*, undergoing the 2s<sup>2</sup>2p<sup>2</sup>(<sup>3</sup>P)3p → 2s<sup>2</sup>2p<sup>2</sup>(<sup>3</sup>P)3s (746.8 nm) transition, to excited Ar\* undergoing the 3s<sup>2</sup>3p<sup>5</sup>(<sup>2</sup>P<sub>1/2</sub><sup>o</sup>)4p → 3s<sup>2</sup>3p<sup>5</sup>(<sup>2</sup>P<sub>1/2</sub><sup>o</sup>)4s (750.4 nm) transition and then calculate the density of ground state N in the system based on the known density of the ground state Ar population. This technique has been used previously in Ar/N<sub>2</sub> mixtures in ICPs by this author<sup>17</sup> and by Czerwiec *et al.*<sup>29</sup> We have chosen the Ar\* 750.4 nm line and the N\* 746.8 nm line because all states are predominantly populated by direct excitation from their respective ground states and should thus be relatively unperturbed by changes in the low energy (<5 eV) electron population.<sup>29</sup> In addition, the excited states from which the transitions originate have similar thresholds [13.48 eV for the Ar-3s<sup>2</sup>3p<sup>5</sup>(<sup>2</sup>P<sub>1/2</sub><sup>o</sup>)4p state and 11.9 eV for the N-2s<sup>2</sup>2p<sup>2</sup>(<sup>3</sup>P)3p state]. This makes the excitation rates less sensitive to the portion of the electron energy distribution function

(EEDF) near the threshold energies. Since positioning of the Langmuir probe for electron temperature measurements was limited to the region outside the ICP orifice, estimates of the electron temperature within the ICP were based on the work by Kang *et al.*,<sup>12</sup> and used to calculate excitation rate constants. Further details on this measurement technique can be found elsewhere.<sup>17,30</sup>

#### D. Langmuir probe

Measurements of plasma density,  $n_e$ , electron temperature,  $T_e$ , plasma potential, and  $V_p$  were performed using an RF compensated Langmuir probe. Voltage sweeps and current monitoring were performed using a Keithley 2400 source meter with data acquisition controlled using a custom LABVIEW interface. The position of the Langmuir probe in the system is shown in Fig. 1. The probe was kept small to minimize perturbation to the plasma. Single bore 1.27 mm OD alumina tubing was used for the end of the Langmuir probe with the tip consisting of 10 mm of 0.1 mm diameter platinum wire. Further details on the probe setup can be found elsewhere.<sup>30</sup>

#### E. RF power monitoring

For the G2, the RF power to the ICP was monitored using a combination of the inline RF power meter in the amplifier unit and a Rogowski coil (Tektronix TRCP 0600 Current Transducer) to independently monitor current. These diagnostics allow for the measurement of the RF power absorbed by the plasma,  $P_{pl}$ , using the method outlined by Godyak and Alexandrovich.<sup>31</sup> Briefly, measuring  $P_{pl}$  requires measuring the ratio of the RF antenna current with the plasma ignited,  $I_c$ , to the RF antenna current without the plasma ignited,  $I_{co}$ . Plasma ignition in this case is controlled by modulating gas flow into the ICP. The power lost to the antenna with the plasma ignited,  $P_A$ , is found via the following

$P_A = P_{A0}(I_c/I_{co})$ . In this equation,  $P_{A0}$  represents the power lost to the antenna in the absence of plasma. Using the fact that the total power,  $P_T = P_{pl} + P_A$ , allows for the calculation of the power transfer efficiency to the plasma,  $\eta = P_{pl}/P_T$ . Since  $\eta$  is dependent on the electron heating mode, monitoring  $\eta$  in relation to process parameters provides a means to observe changes in the electron heating mode as process parameters are varied.

In addition to the power and current monitoring outlined above, the voltage on the antenna coil nearest the ICP orifice was also monitored using a high frequency voltage probe (1000:1 Tektronix 6015). The time dependent measurements were all collected using a Tektronix MDO 34, 200 MHz oscilloscope. Unfortunately, due to the smaller size of the G1 system and the assembly of its RF shielding, it was not possible to attach these diagnostic tools to the G1 antenna without the risk of damaging the unit. A diagram of this setup is shown in Fig. 2 along with a comparison between changes in  $\eta$  and total wavelength integrated emission from the ICP. These data illustrate how total emission and  $\eta$  are correlated as electron heating mode changes in an ICP.

### III. EXPERIMENTAL RESULTS AND DISCUSSION

In this section, we explore the effect of varying process control parameters (varying neutral pressure as well as the total and relative mass flow rate) on the plasma properties (relative neutral density, gas temperature, electron density,  $n_e$ , electron temperature,  $T_e$ , and plasma potential,  $V_p$ ) of the remote ICP sources. For select cases, the spatial variation of the aforementioned plasma properties is also examined. The effects of varying these process control parameters on the plasma properties are then discussed in terms of their relationship to power coupling and the respective influence of the plasma-surface interactions that drive thin-film growth and film properties during the plasma step during PEALD processes.

25 April 2024 03:49:28

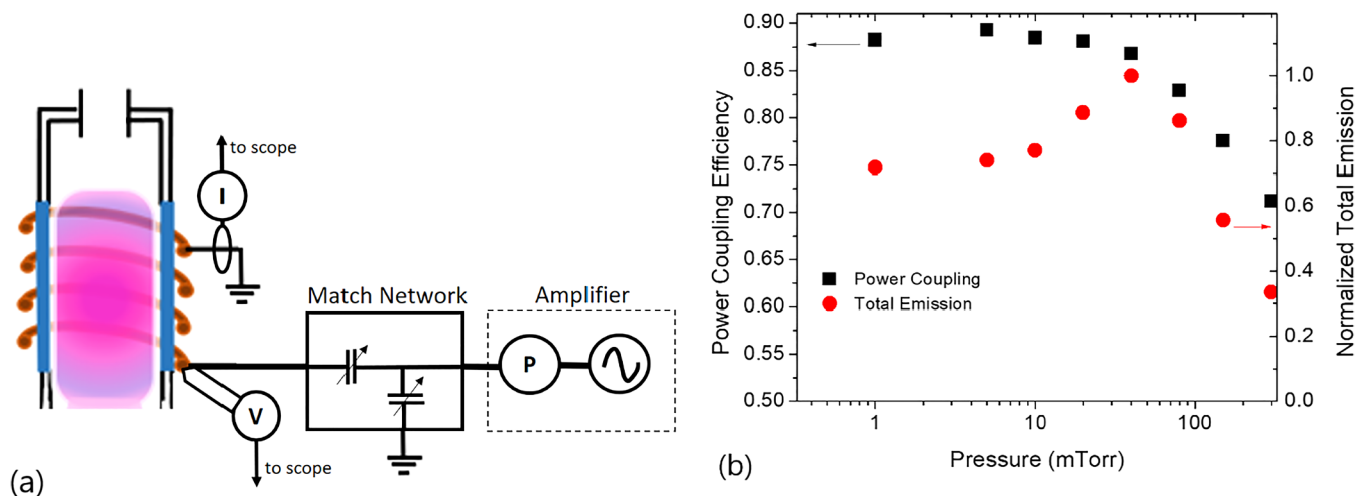


**FIG. 2.** (a) RF power measurement setup for the G2 setup with V indicating the location of the high speed voltage probe, I indicating the location of the Rogowski coil, and P indicating the built-in RF power monitor on the amplifier unit. (b) Comparison of power coupling efficiency,  $\eta$ , to total emission from the ICP as a function of pressure with the reduction in emission at high pressures being correlated with a reduction in  $\eta$ .

### A. Optical emission spectroscopy measurements

The optical characterization of the plasma sources is an effective way to recognize changes in plasma electron heating modes, as the mode transitions between E-mode and H-mode are accompanied by changes in light emission intensity and color. These changes, when monitored with optical emission spectroscopy, can inform the user about the relative concentrations of reactive and excited neutrals within the plasma source. In  $N_2$  containing plasmas, the relative concentration of atomic N in the gas phase is of particular interest. A volume-averaged measure of this density can be found using the actinometrical procedures outlined above in the experimental details, Sec. II C.

In this section, the effects of varying pressure, varying flow fractions of Ar and  $N_2$ , and varying total flow within the ICP are examined in terms of how these process parameters affect the atomic N density generated within the ICP source. The G1 and G2 configurations are also compared in this context. In Fig. 3, the total emission intensity of the ICP sources is measured as a function of operating pressure for a high  $N_2$  flow fraction ( $\approx 90\%$   $N_2$  by flow in all cases). The G1 source exhibited a sharp reduction in emission as pressure is increased between 50 and 100 mTorr when the total flow into the ICP was 33 SCCM. Indeed, for this low flow condition, over this relatively modest range of pressures, the emission intensity drops by  $\approx 20\times$  for this lower mass flow condition, a clear indicator of an H-mode to E-mode transition. In contrast, the G1 source did not exhibit this sharp mode transition when the total mass flow rate was higher, 110 SCCM. However, the total emission from the ICP remained comparatively low over the entire pressure range examined for the 110 SCCM mass flow condition. This seems to indicate that for these high  $N_2$  flow fractions the ability of

the G1 ICP source to reach H-mode is dependent on the mass flow rate. A similar sharp transition from H-mode to E-mode with increasing pressure was not observed in the G2 configuration. Rather, the emission first rises with increasing pressure before gradually falling at pressures above 75–100 mTorr for both of the flow conditions examined (33 and 110 SCCM).

Figure 4 shows the atomic N density in both the G1 and G2 sources as a function of pressure, illustrating their differing behavior. Examining atomic N density in the G1 source again shows a significant difference between the low flow and high flow cases with the low flow case exhibiting the highest atomic N density at low pressures ( $<100$  mTorr), with a notable  $10\times$  drop in atomic N density between 50 and 100 mTorr. This contrasts with the high flow G1 case and the G2 case where the highest atomic N densities are measured at the highest pressures ( $>100$  mTorr). The difference in behavior between the low flow G1 condition and the high flow G1 and G2 conditions indicates that gas residence time could play a role in the H-mode behavior observed for the low flow condition of the G1 source. This would make sense as a lower mass flow rate through the ICP source would allow more time for the high energy electrons to interact with a given quantity of gas.

Figure 5 shows the atomic N density in the G2 source when the pressure is held constant at 30 mTorr and the mass flow rate is varied. Interestingly, only gradual changes are observed in the atomic N density. In addition, there is no abrupt change in total photon emission from the G2 ICP, indicating that no heating mode transitions occur with varying mass flow in the G2 configuration. However, the data also show that at lower mass flow rates higher densities of atomic N are produced. This is again consistent with the notion that longer gas residence time within the ICP allows for

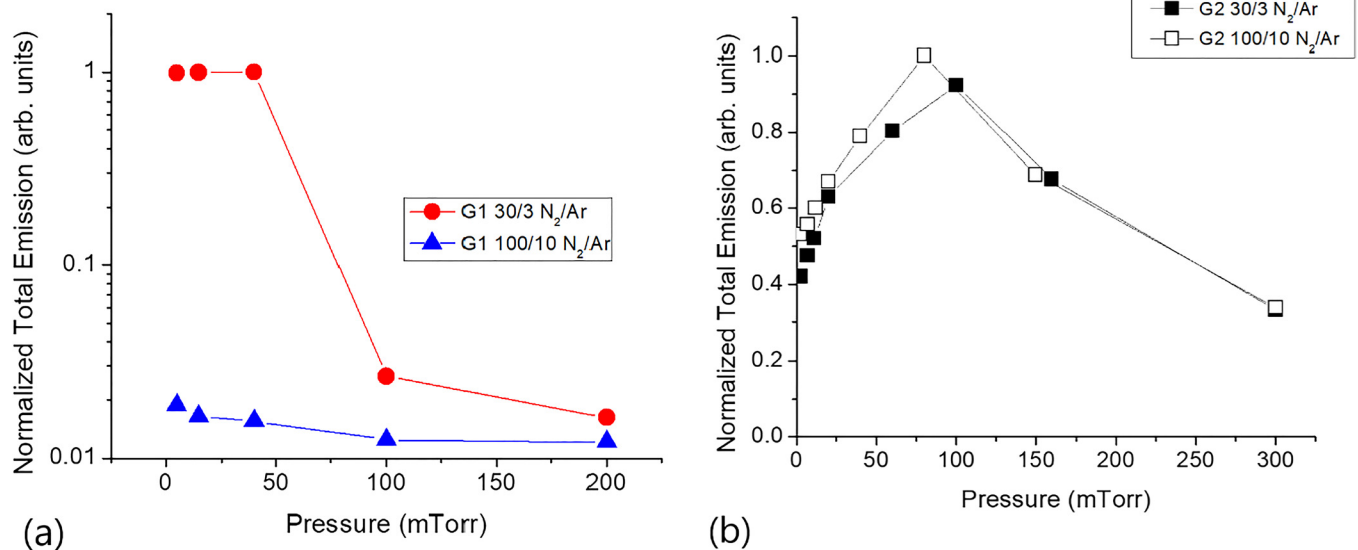
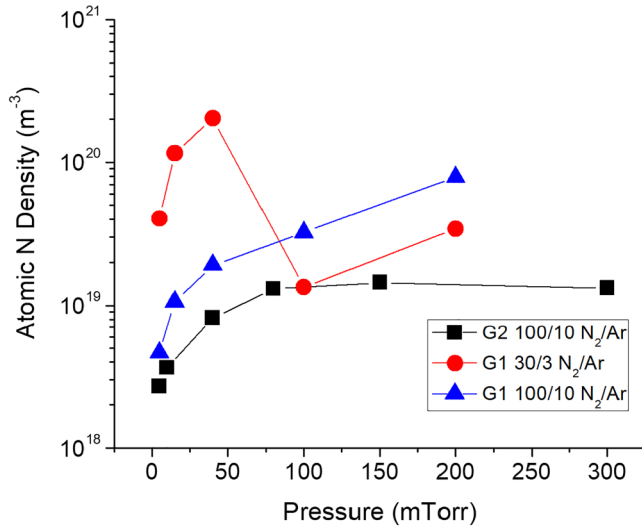


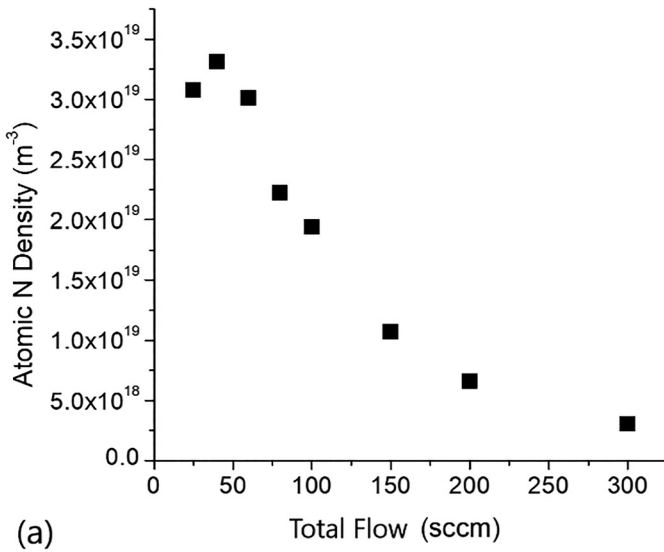
FIG. 3. Normalized total emission measurements from the Fiji G1 (a) and Fiji G2 (b). The ICPs were operated at two flow conditions 30 SCCM  $N_2/3$  SCCM Ar and 100 SCCM  $N_2/10$  SCCM Ar. In both the G1 and G2 cases, the data are normalized to the maximum emission observed across both flow regimes. Note the abrupt change in total emission observed between 50 and 100 mTorr in the G1 at low flow (33 SCCM) is indicative of an H- to E-mode transition.

25 April 2024 03:49:28



**FIG. 4.** Atomic N density measured via actinometry as a function of pressure for both the G1 and G2 sources. The G1 data are shown for both a high mass flow (110 SCCM) and a low mass flow (33 SCCM) condition. The G2 data are shown only for the high mass flow (110 SCCM) condition. Note the abrupt change in the N density in the G1 at low flows (33 SCCM) corresponds to a similar change in total emission shown in Fig. 3.

more effective dissociation of N<sub>2</sub>. In Fig. 5, the mass flow ratio of N<sub>2</sub> to Ar was held constant at 10. Under these low Ar content conditions, the dissociation fraction of the gas generally varied between ≈3% at the lowest mass flow rates to ≈0.3% at the highest mass



flow rates. It is also notable that across these changes in mass flow rate RF power coupling to the plasma remained effectively unchanged with power coupling efficiency decreasing by only 2% between the low flow and high flow cases.

As Ar content within the plasma is varied, the atomic N density and the dissociation fraction of N<sub>2</sub> were found to increase significantly with increasing Ar flow fraction. This effect is illustrated in Fig. 6(a), which shows the atomic N density within the G1 system and G2 system as a function of N<sub>2</sub>/(N<sub>2</sub> + Ar) flow fraction. The G1 data were taken at a total flow rate of 175 SCCM, whereas the G2 data were taken at a slightly higher total flow rate of 200 SCCM. In the case of the G1 data, the atomic N 747 nm emission line became too dim to measure at N<sub>2</sub> flow fractions greater than 25%. This is consistent with previous results<sup>17</sup> and indicates an H-mode to E-mode transition with increasing N<sub>2</sub> flow fraction in the G1 system. The G2 system also showed decreasing atomic N density with increasing N<sub>2</sub> flow fraction but the decrease was more gradual and the 747 nm emission line from N was detectable even at high N<sub>2</sub> flow fractions. In Fig. 6(b), the variation of atomic N density with pressure is shown for two bounding cases of high N<sub>2</sub> flow fraction (90% by flow) and low N<sub>2</sub> flow fraction (12% by flow). It is clear from the figure that atomic N density is greater and increases much more rapidly with pressure when there is high Ar content in the ICP. This is consistent with previous observations and modeling of ICP behavior in Ar/N<sub>2</sub> mixtures<sup>12,17,30</sup> and is an important consideration if one wishes to control atomic N flux at a downstream growth surface.

The OES data compiled in this section show both similarities and differences between the G1 and G2 sources for the operating conditions examined in this work. Both sources exhibit increased atomic N production at lower total mass flow rates with the G1 source showing a dramatic increase indicative of an E-mode to

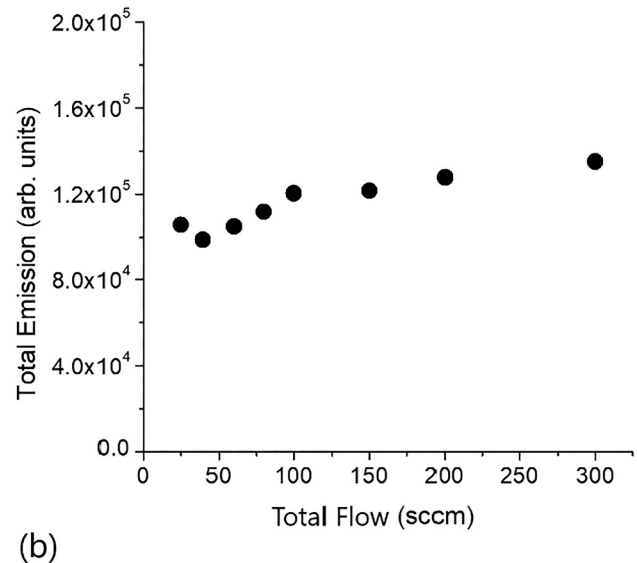


**FIG. 5.** G2 source (a) atomic N density as a function of mass flow at a background pressure of 30 mTorr and an N<sub>2</sub>/(N<sub>2</sub> + Ar) flow ratio of 0.9. (b) Total emission intensity as a function of mass flow rate for the same conditions.

25 April 2024 03:49:28

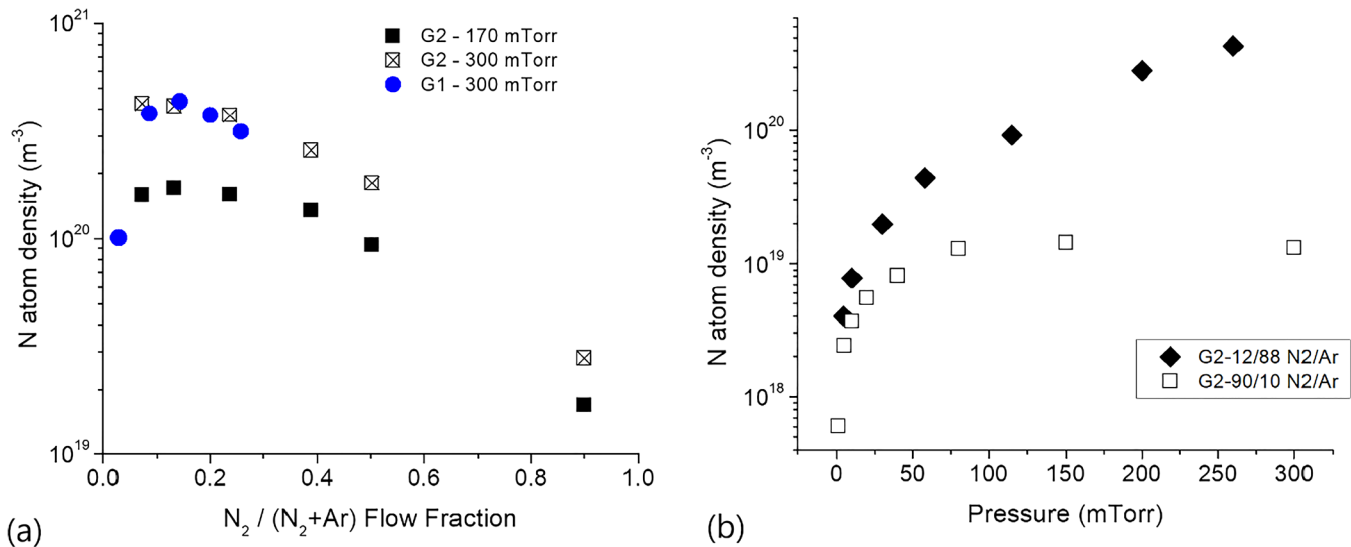


**FIG. 6.** (a) Atomic N density within the G1 system and G2 system as a function of  $\text{N}_2/(\text{N}_2 + \text{Ar})$  flow fraction. The G1 data were taken at a total flow rate of 175 SCCM, and the G2 data were taken at a total flow rate of 200 SCCM. (b) Atomic N density as a function of pressure for a low  $\text{N}_2$  condition (12% by flow) and a high  $\text{N}_2$  condition (90% by flow). The total flow in both cases was 100 SCCM.

H-mode transition as mass flow rate decreased and pressures were below 100 mTorr. Also similar was the atomic N production as a function of the  $\text{N}_2/\text{Ar}$  flow fraction at high total flow and pressure, where both sources showed significantly increased atomic N production at low  $\text{N}_2/\text{Ar}$  flow fractions. Again, however, the G1 source exhibited a large increase in N atom density as relative  $\text{N}_2$  flow decreased below 30%, suggesting a change from E-mode to H-mode. The G2 source did not exhibit the jump in light emission associated with such a heating mode change. This trend was also observed in the pressure scan data where an abrupt E-mode to H-mode transition was observed with increasing total pressure in the G1 source but only a gradual change was observed with increasing pressure for the G2 case. In Sec. III B, the charged particle characteristics of these two sources are examined for the same set of process parameters.

The OES data compiled in this section show both similarities and differences in the production of atomic nitrogen between the G1 and G2 sources for the operating conditions examined in this work. Broadly, the N density in both sources is found to increase when increasing operating pressure, decreasing total flow, and decreasing the nitrogen flow fraction. However, the relative increase and/or decrease can be strongly impacted in the G1 due to heating mode changes. For example, an abrupt order of magnitude decrease in atomic N density is observed when the pressure increases between 50 and 100 mTorr at low total flow rates. A similarly abrupt change is seen in the G1 when decreasing the nitrogen flow fraction below 30% at high pressures. While the magnitude of the atomic nitrogen density can be varied significantly in the G2 source over the range of parameters explored here, there were no abrupt changes like those observed in the G1. Although the downstream emission in the system was not sufficient to reliably

determine the amount of atomic nitrogen, it is reasonable to assume an increase or decrease near the exit of the source will lead to a corresponding change in density near a substrate in configurations used for processing.

## B. Langmuir probe measurements

Using an RF compensated Langmuir probe allows for changes to plasma potential and plasma density to be examined as process parameters are varied. These two plasma parameters determine the maximum ion energy and the flux of ions at surfaces, which are invaluable for understanding the changes observed in film growth as a function of varying process conditions.

In this section, we again begin with a comparison of the G1 and G2 sources as pressure is varied within the reactor. In Fig. 7, it is shown that the G2 source generates significantly different plasma densities and plasma potentials downstream of the ICP (location 200 mm downstream of ICP orifice) compared to the G1 source. It is also notable that while there are some slight differences in density and plasma potential between the low flow (30 SCCM  $\text{N}_2/3$  SCCM Ar) and high flow (100 SCCM  $\text{N}_2/10$  SCCM Ar) conditions, there were no abrupt changes in downstream plasma conditions with increasing pressure. This contrasts with the observations discussed earlier regarding the upstream atomic N production within the ICP, suggesting that mode changes impact the charged particle characteristic near the substrate less.

The general trends with increasing pressure show a decreasing plasma density and increasing plasma potential. This is consistent with previous observations of remote, capacitively coupled plasma (CCP) systems,<sup>32–34</sup> which indicated that while the mean ion energy decreases at grounded surfaces, due to increasing



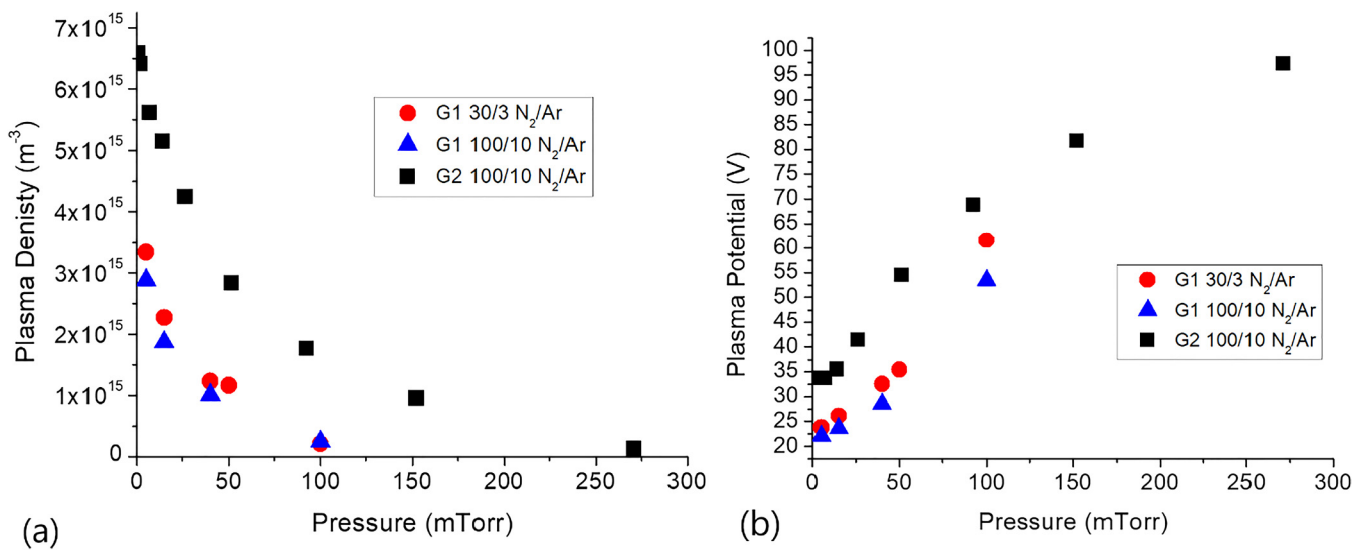


**FIG. 7.** (a) Plasma density as a function of pressure at 200 mm downstream from ICP orifice. G1 data taken at two flow conditions (30 SCCM N<sub>2</sub>/3 SCCM Ar and 100 SCCM N<sub>2</sub>/10 SCCM Ar), and G2 data taken at one flow condition (100 SCCM N<sub>2</sub>/10 SCCM Ar). (b) Plasma potential as a function of operating pressure at 200 mm downstream from ICP orifice for the same flow conditions.

collisionality within the sheath, the maximum ion energy can increase with increasing pressure. This effect is driven by a decrease in current flow to the larger grounded electrode surface in the asymmetric CCP system,<sup>4</sup> which tends to decrease the asymmetry of current flow in the system and thus leads to an increased average plasma potential. This is due to the fact that RF oscillations are shared between the active and grounded electrodes in proportion to the capacitance of the plasma sheaths at these electrodes, which is determined mainly by the surface areas of the grounded and active electrodes. This interpretation is consistent with increasing plasma potential observed as pressure increases in the remote ICP configuration of this work, where capacitive coupling is playing an important role in the plasma behavior downstream from the ICP. Here, however, the small orifice connecting the ICP to the main chamber acts as a virtual driven electrode and the downstream chamber walls form the ground electrode. The capacitance of the ICP antenna promotes plasma potential oscillations within the ICP tube, which acts as a small, highly asymmetric powered electrode. Indeed, the hypothesis that the ICP antenna promotes an asymmetric capacitively coupled voltage oscillation in the downstream plasma is consistent with the lower average plasma potentials measured in the G1 system. This would be expected since the surface area encompassed by the G1 antenna is significantly smaller than the surface area encompassed by the G2 antenna and would thus lead to an even more asymmetric electrode configuration and, thus, RF potential at grounded electrodes. It is interesting to note that in addition to the effects described above from decreased current flow to grounded surfaces, there are also changes to the RF voltage on the ICP antenna to consider. From the voltage probe measurements described in Sec. II E, it was found that increasing pressure had a significant effect on the antenna voltage measured near the ICP

orifice. An increase in voltage amplitude from 750 to 1325 V was observed as pressure was increased from 5 to 270 mTorr. While much of this voltage change will be dropped across the wall of the dielectric tube, some will influence the plasma potential oscillations within the ICP. This could consequently increase the RF potential oscillations in the downstream portion of the reactor, which would further increase the average plasma potential in that part of the system.

In Fig. 8, the spatial distribution of plasma density and plasma potential is shown for the case of 100 mTorr and mass flow conditions of (100 SCCM N<sub>2</sub>/10 SCCM Ar). Here again, a notable difference is observed between G1 and G2 cases, with the G2 source producing about 5–10× higher plasma density at all locations and a significantly higher plasma potential. While the ion energy distribution will likely be substantially degraded by ion–neutral collisions at these pressures, such a difference in plasma potentials could still have an effect on the high energy tail of the ions, which could have effects on material growth. The different radii of the G1 and G2 ICP sources likely drive these significant differences in plasma parameters between the two sources, as the G1 source with its smaller radii will lose charged particles to the tube walls much more rapidly than the larger radii G2 source. This reduced density near the ICP orifice, in the G1 case, then propagates lower density plasma into the downstream portion of the reactor. In addition, the lower plasma potential in the G1 case is likely from the smaller diameter orifice, which provides a more asymmetric ratio between powered and grounded surface areas within the reactor.

While many PEALD processes are performed at reactor pressures of 100 mTorr and higher, the growth of crystalline films is often performed at low pressures where high fluxes of ions are incident on the substrate surface. To examine these conditions, spatial

25 April 2024 03:49:28

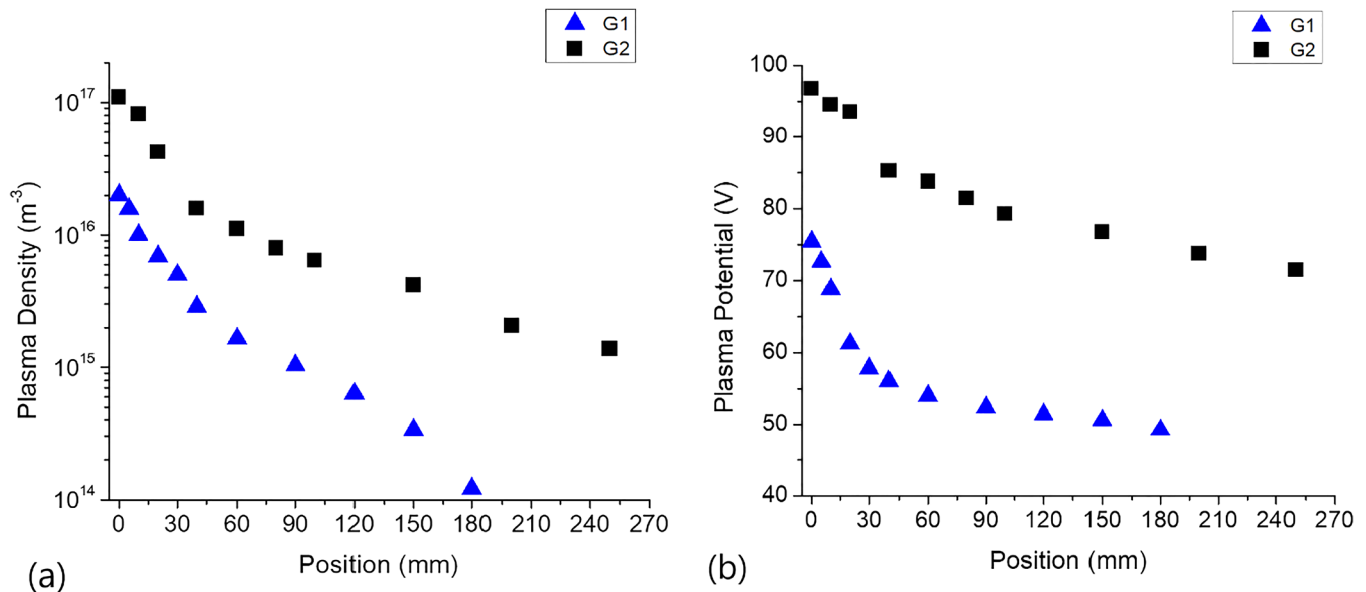


**FIG. 8.** (a) Plasma density as a function of position along the axis of the diagnostic reactor downstream from the orifice of the ICP (position = 0 mm). (b) Plasma potential as a function of position along the axis of the diagnostic reactor downstream from the orifice of the ICP. All measurements were taken at 100 mTorr pressure and a mass flow of 100 SCCM  $\text{N}_2$  and 10 SCCM Ar.

scans were performed at 5 mTorr reactor pressure with both the G1 and G2 sources affixed to the reactor. In these measurements, shown in Fig. 9, it is again apparent that the G1 source produces lower downstream plasma density and plasma potential than the G2 source. In Fig. 9, the effect of varying mass flow is also examined in the context of downstream plasma density and potential. Here, the spatial profiles of density and potential are shown for two different mass flow rates with a low flow (30 SCCM  $\text{N}_2$ /3 SCCM Ar) and high flow (100 SCCM  $\text{N}_2$ /10 SCCM Ar) condition. While there is little difference between the low flow and high flow conditions for the plasma density profiles in the G2 case, it is notable that the G1 configuration seems to produce slightly higher plasma density near the ICP orifice in the low flow condition compared with the high flow condition. This could be an effect of the H-mode to E-mode transition that occurs with an increasing mass flow rate in the G1 source, as previously discussed in Sec. III A. Interestingly, when plasma potential is examined, it is found that the G1 plasma potential profiles change little between the high flow and low flow conditions, whereas the G2 plasma potential profiles are nearly 5 V higher in the low flow conditions compared to the high flow conditions. At these pressure conditions, the ion energy distribution at a downstream surface will surely trend higher with this change in plasma potential. In turn, these results indicate a potential means through which changing mass flow rate can affect film growth and perhaps even film crystallization through effects on the ion energy at surfaces.

In Fig. 10, the effect of mass flow on plasma potential and density downstream from the G2 source is examined more closely. In Fig. 10, flow rates from 20 to 140 SCCM are examined with the

pressure held constant at 5 mTorr and gas flow fractions kept constant at 90%  $\text{N}_2$  and 10% Ar. All the data were taken at 200 mm from the ICP orifice. It was found that while plasma density remained essentially constant across this range in mass flow rates, plasma potential varied between 32 V at 140 SCCM and 40 V at 20 SCCM. Previously, this range in flows was found to affect the atomic N density and dissociation fraction of the background gas within the ICP. It is unclear how this effect is manifesting a change in plasma potential downstream from the G2 source. It does not appear that power-coupling efficiency to the plasma in the source plays a role here as  $\eta$  varies by only 2% between the low flow and high flow conditions. It is notable that mass flow rate had a small effect on antenna RF voltage amplitude (increasing from 1650 to 1740 V from 20 to 140 SCCM) but it is unclear whether or not this modest change in antenna voltage could drive the downstream changes in plasma potential observed in the G2 system.

In Figs. 11 and 12, the effect of varying the flow fraction of the Ar and  $\text{N}_2$  is examined on the plasma parameters measured downstream from the G2 source. In Fig. 11, the variation in plasma density [Fig. 11(a)] and plasma potential [Fig. 11(b)] with pressure is shown for two flow fractions of Ar and  $\text{N}_2$ : a high  $\text{N}_2$  flow fraction case with 90%  $\text{N}_2$  by flow and a low  $\text{N}_2$  flow fraction case with 12%  $\text{N}_2$  by flow. In Fig. 11(a), plasma density is somewhat elevated in the low  $\text{N}_2$  flow fraction case relative to the high  $\text{N}_2$  flow fraction case, although the difference is most pronounced at low pressures, at high pressures (>100 mTorr) the difference is likely within measurement error. In Fig. 11(b), plasma potential appears to be markedly higher in the high  $\text{N}_2$  flow fraction case compared to the low  $\text{N}_2$  flow fraction case with this difference becoming more

25 April 2024 03:49:28

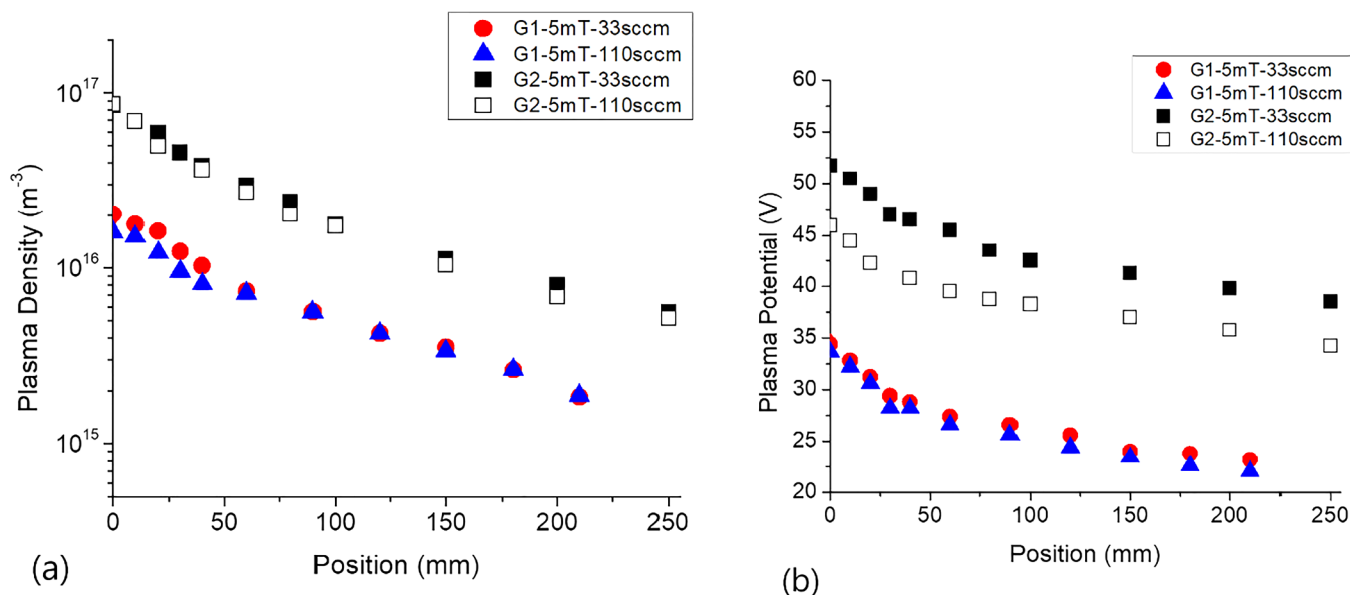


**FIG. 9.** (a) Plasma density as a function of position along the axis of the diagnostic reactor downstream from the orifice of the ICP (position = 0 mm). (b) Plasma potential as a function of position along the axis of the diagnostic reactor downstream from the orifice of the ICP. All measurements were taken at 5 mTorr pressure and mass flow percentages of 90%  $N_2$  and 10% Ar.

pronounced as pressure is increased. For low pressure operation, this will again likely have an effect on the ion energy distribution as maximum ion energies at surfaces are closely tied to the plasma potential. In Fig. 12, the pressure was held fixed at 150 mTorr and

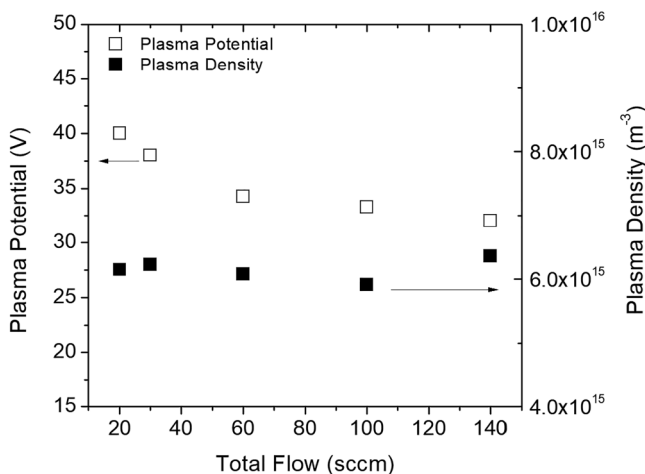


**FIG. 10.** Effect of mass flow on plasma potential and density downstream from the G2 source. Total mass flow rate is varied between 20 and 140 SCCM with the pressure held constant at 5 mTorr and gas flow fractions held constant at 90%  $N_2$  and 10% Ar. All measurements were performed 200 mm from the orifice of the G2 ICP.

the flow ratio  $N_2/(N_2 + Ar)$  was varied by adjusting the mass flow ratios into the reactor while keeping the total mass flow constant. Here again, the plasma potential increases with increasing  $N_2$  content in the reactor while plasma density remains relatively constant. This is consistent with the notion that increased  $N_2$  content within the reactor leads to overall decreased current flow to grounded surfaces within the system and results in a decrease in the asymmetry between the capacitive RF voltage drop at the ICP and RF voltage drop at grounded surfaces elsewhere in the reactor. Since increased  $N_2$  content leads to higher electron-ion recombination within the plasma, it is possible that a more rapid spatial decay of the plasma with distance from the ICP orifice is mediating this reduced current flow to grounded surfaces and thus increased average plasma potential within the reactor.

The Langmuir probe data compiled in this section illustrate a number of important trends in plasma density and plasma potential with varying process parameters. First, with increasing pressure, it was shown that plasma density decreases downstream from the ICP orifice whereas plasma potential increased with increasing pressure. This indicates that chamber pressure is a useful parameter for controlling ion flux at growth surfaces. It is also important to note that while both the G1 and G2 sources exhibited similar trends with pressure, the G2 source generally exhibited substantially higher plasma density and plasma potential downstream from the ICP orifice. We speculate that this is due to changes in the relative plasma fluxes at grounded surfaces downstream from the ICP orifice, and to the ICP orifice. This assumes that capacitive coupling from the ICP antenna to the ICP plasma results in the ICP orifice acting like a powered electrode in an asymmetric CCP

25 April 2024 03:49:28

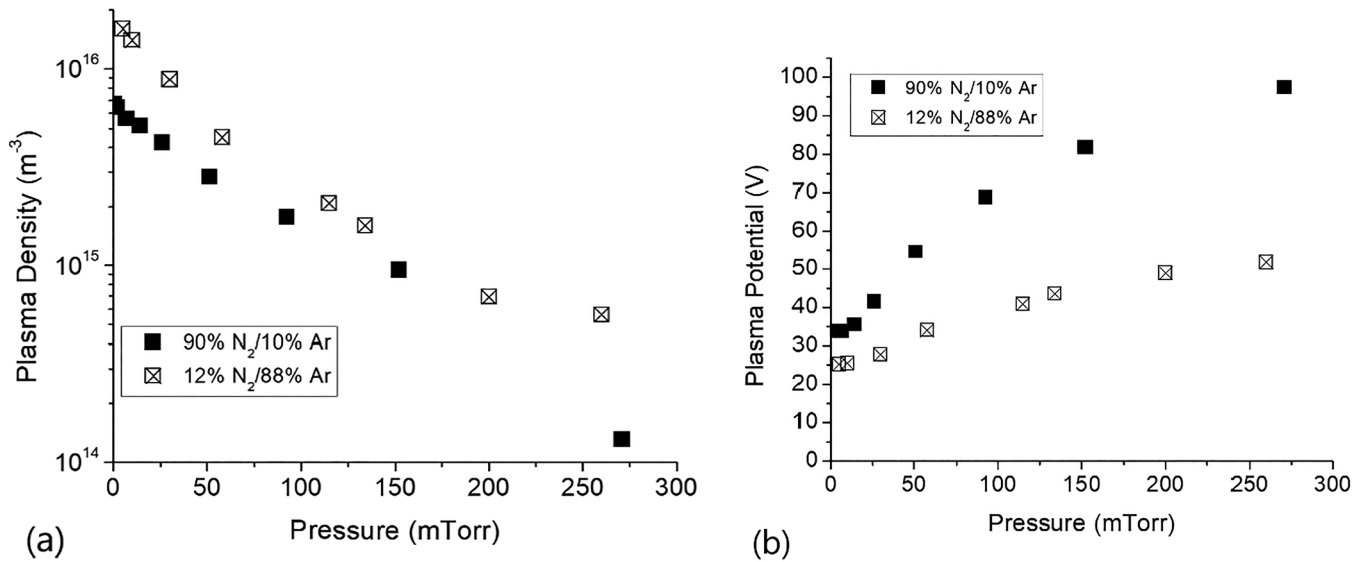


**FIG. 11.** Effect of pressure on plasma potential and density 200 mm downstream from the G2 source. (a) Plasma density as a function of pressure for two flow conditions: a high N<sub>2</sub> flow fraction case with 90% N<sub>2</sub> by flow and a low N<sub>2</sub> flow fraction case with 12% N<sub>2</sub> by flow. (b) Plasma potential as a function of pressure for the same flow conditions.

system. As such, reductions in current flow to the grounded surfaces downstream from the ICP orifice would lead to more symmetric voltage distribution between the grounded and powered sections of the reactor, and an overall increase in average plasma potential. This is an important consideration in circumstances when ion flux at the substrate needs to be carefully controlled.

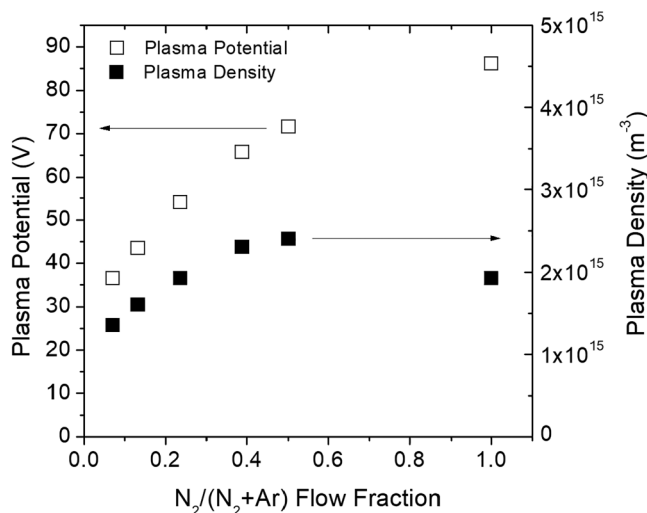


**FIG. 12.** G2 Plasma density and plasma potential as a function of N<sub>2</sub>/(N<sub>2</sub> + Ar) flow fraction, all measurements taken at 200 mm distance from the ICP orifice. Reactor pressure was held fixed at ≈150 mTorr for all measurements.

While the aforementioned trends in pressure were somewhat expected, a more surprising finding was the effect of varying mass flow rate on the downstream plasma potential and density. While density remained relatively fixed across variable flow mass flow rates, plasma potential was significantly affected by adjustments in the mass flow rate into the system. In fact, changes in plasma potential on the order of 5–10 V were observed as the mass flow rate was varied between 20 SCCM through 140 SCCM. This change is significant in the context of atomic precision processing, especially for the growth of materials sensitive to ion damage. It is notable that these changes in the plasma potential were far more pronounced in the G2 system compared to the G1 system. Since no significant change in RF power coupling was observed with mass flow rate, and plasma density was generally unchanged with varying mass flow rate, it is less clear what drives this change in plasma potential.

Finally, plasma density and plasma potential were also found to vary significantly as a function of N<sub>2</sub>/(N<sub>2</sub> + Ar) flow fraction. At high N<sub>2</sub> flow fractions, plasma potential was significantly higher (≈2× higher) than at low N<sub>2</sub> flow fractions. This was attributed to the effect of a higher electron-ion recombination rate with increasing N<sub>2</sub> flow fraction and thus reduced RF current flow to grounded surfaces downstream from the ICP orifice. This effect leads to a reduction in the overall current flow asymmetry between grounded and powered surfaces within the downstream region of the reactor and thus an increase in the plasma potential in this part of the reactor.

#### IV. CONCLUSIONS

This work has focused on examining two important features of PEALD reactor operation in Ar/N<sub>2</sub> mixtures. First, it examined

25 April 2024 03:49:28

how atomic nitrogen generation within the ICP source was affected by changes in neutral pressure, total gas flow, and relative gas flows of Ar and N<sub>2</sub>. Second, it examined how charged particle characteristics in the downstream section of a PEALD reactor respond to changes in these same critical operating parameters. In addition, the effect of varying these operating parameters was examined for two commonly used ICP plasma sources, a Veeco G1 ICP and Veeco G2 ICP. The main differences between these two sources are their dimensions and antenna designs. The volume of the G2 is greater than the G1 and the G2 has a larger exit orifice at the source–chamber interface. The G2 antenna has more turns and is longer than the G1 antenna, while the G1 antenna is grounded near the exit orifice and the G2 antenna is powered near the exit orifice. The findings of this work are outlined below.

- (1) With increasing pressure in a gas mixture of 90% N<sub>2</sub> by flow, the G2 source generally exhibited an increasing atomic N density with increasing pressure, although atomic N density increased sublinearly. Conditions with higher Ar content by flow exhibited more effective dissociation of N<sub>2</sub> with atomic N density increasing more rapidly with pressure under high Ar content conditions (88% Ar by flow).
- (2) With increasing pressure in a gas mixture of 90% N<sub>2</sub> by flow and 33 SCCM total mass flow rate, the G1 source exhibited a H- to E-mode transition between 50 and 100 mTorr resulting in very high (>10<sup>20</sup> m<sup>-3</sup>) atomic N density at pressures below 100 mTorr and generally lower atomic N density (<10<sup>20</sup> m<sup>-3</sup>) at higher pressures.
- (3) In both the G1 and G2 sources, increasing pressure resulted in reduced plasma density downstream from the ICP orifice at measurement positions near the nominal location of growth substrate. Increasing pressure also resulted in increased plasma potential at this location, although this increased plasma potential would generally not result in increased mean ion energy due to increasing ion neutral collisions at increased neutral pressures.
- (4) As the total mass flow rate within the reactor was varied, decreasing mass flow generally resulted in increased atomic N density in both the G1 and G2 sources. In the G1 source, there was a mode transition between E- and H-mode observed with a decreasing mass flow rate that led to a large and rapid increase in atomic N generation. The G2 source exhibited a more gradual increase in atomic N as mass flow rate was decreased. These findings indicate that increased gas residence time within the ICP leads to higher dissociation fractions of N<sub>2</sub>.
- (5) As the total mass flow rate within the reactor was varied, decreasing mass flow generally resulted in relatively constant plasma density at distances 200 mm downstream from the ICP orifice. This was the case in both the G1 and G2 configurations. Where the G1 configuration exhibited relatively little change in plasma potential with varying mass flow rate, the G2 configuration exhibited a 5–10 V increase in plasma potential as mass flow rate was decreased from 140 to 20 SCCM.
- (6) As N<sub>2</sub>/(N<sub>2</sub> + Ar) flow fraction was varied, atomic N density was found to decrease with increasing N<sub>2</sub> flow fraction in both

the G1 and G2 sources. In the G1 source at high pressure (≈300 mTorr), an H to E-mode transition was observed at N<sub>2</sub>/(N<sub>2</sub> + Ar) flow fractions >0.25. In the G2 source, the reduction in atomic N density was gradual with increasing N<sub>2</sub>/(N<sub>2</sub> + Ar) flow fraction.

- (7) Increasing N<sub>2</sub>/(N<sub>2</sub> + Ar) flow fraction resulted in relatively constant plasma density at 200 mm from the G2 ICP orifice; however, plasma potential was found to increase significantly (from 35 to 85 V) as N<sub>2</sub>/(N<sub>2</sub> + Ar) flow fraction was increased. These measurements were performed at high pressure (150 mTorr).
- (8) Overall, the G1 source exhibited lower plasma density and plasma potential compared with the G2 source for measurements performed at all locations within the reactor and at all conditions.
- (9) In general, the effects of capacitive coupling from the ICP antenna appear to play an important role in the downstream plasma potential in both the G1 and G2 systems. Particularly, for low pressure operation, these capacitive coupling effects could lead to elevated ion energies at the substrate. For certain material systems, these effects may be undesirable. As such, ICP antenna designs that minimize antenna capacitive coupling<sup>31</sup> could be useful in mitigating these capacitive coupling effects and reducing downstream plasma potential.

## ACKNOWLEDGMENTS

This work was supported by the Naval Research Laboratory Base Program.

## AUTHOR DECLARATIONS

### Conflict of Interest

The authors have no conflicts to disclose.

## Author Contributions

**David R. Boris:** Conceptualization (lead); Data curation (lead); Formal analysis (lead); Investigation (lead); Methodology (lead); Resources (equal); Writing – original draft (lead); Writing – review & editing (equal). **Michael J. Johnson:** Data curation (equal); Investigation (equal); Writing – review & editing (equal). **Jeffrey M. Woodward:** Resources (equal); Writing – review & editing (equal). **Virginia D. Wheeler:** Resources (equal); Writing – review & editing (equal). **Scott G. Walton:** Conceptualization (equal); Funding acquisition (lead); Project administration (equal); Supervision (equal); Writing – review & editing (lead).

## DATA AVAILABILITY

The data that support the findings of this study are available from the corresponding author upon reasonable request.

## REFERENCES

- <sup>1</sup>H. B. Profijt, S. E. Potts, M. C. M. van de Sanden, and W. M. M. Kessels, *J. Vac. Sci. Technol., A* **29**, 050801 (2011).
- <sup>2</sup>H. C. M. Knoops, T. Faraz, K. Arts, and W. M. M. Kessels, *J. Vac. Sci. Technol., A* **37**, 030902 (2019).

- <sup>3</sup>D. R. Boris *et al.*, *J. Vac. Sci. Technol., A* **38**, 040801 (2020).
- <sup>4</sup>M. A. Lieberman and A. J. Lichtenberg, *Principles of Plasma Discharges and Materials Processing*, 2nd ed. (Wiley, Hoboken, NJ, 2005).
- <sup>5</sup>U. Kortshagen, N. D. Gibson, and J. E. Lawler, *J. Phys. D: Appl. Phys.* **29**, 1224 (1996).
- <sup>6</sup>P. Kempkes, S. V. Singh, C. Pargmann, and H. Soltwisch, *Plasma Sources Sci. Technol.* **15**, 378 (2006).
- <sup>7</sup>C. S. Corr *et al.*, *Plasma Sources Sci. Technol.* **21**, 055024 (2012).
- <sup>8</sup>Y. W. Lee, H. L. Lee, and T. H. Chung, *J. Appl. Phys.* **109**, 113302 (2011).
- <sup>9</sup>H. Lee, J. Lee, and C. Chung, *Phys. Plasmas* **17**, 033506 (2010).
- <sup>10</sup>V. A. Godyak, *Plasma Sources Sci. Technol.* **20**, 025004 (2011).
- <sup>11</sup>M. S. Barnes, J. C. Foster, and J. H. Keller, *Appl. Phys. Lett.* **62**, 2622 (1993).
- <sup>12</sup>N. Kang *et al.*, *Plasma Sources Sci. Technol.* **20**, 045015 (2011).
- <sup>13</sup>Y. Mitsui and T. Makabe, *Plasma Sources Sci. Technol.* **30**, 023001 (2021).
- <sup>14</sup>A. Mukherjee *et al.*, *Plasma Sources Sci. Technol.* **32**, 085004 (2023).
- <sup>15</sup>H. Li *et al.*, *J. Appl. Phys.* **121**, 233302 (2017).
- <sup>16</sup>Wei Yang *et al.*, *Plasma Sources Sci. Technol.* **27**, 075006 (2018).
- <sup>17</sup>D. R. Boris *et al.*, *J. Vac. Sci. Technol., A* **36**, 051503 (2018).
- <sup>18</sup>D. R. Boris *et al.*, *J. Vac. Sci. Technol., A* **37**, 060909 (2019).
- <sup>19</sup>V. A. Godyak, R. B. Piejak, and B. M. Alexandrovich, *Plasma Sources Sci. Technol.* **11**, 525 (2002).
- <sup>20</sup>T. Faraz *et al.*, *Plasma Sources Sci. Technol.* **28**, 024002 (2019).
- <sup>21</sup>V. D. Wheeler *et al.*, *Chem. Mater.* **32**, 1140 (2020).
- <sup>22</sup>M. Legallais *et al.*, *ACS Appl. Mater. Interfaces* **12**, 39870 (2020).
- <sup>23</sup>H. C. M. Knoop *et al.*, *ACS Appl. Mater. Interfaces* **7**, 19857 (2015).
- <sup>24</sup>M. Ziegler *et al.*, *Supercond. Sci. Technol.* **26**, 025008 (2013).
- <sup>25</sup>T. Faraz *et al.*, *ACS Appl. Mater. Interfaces* **10**, 13158 (2018).
- <sup>26</sup>J. R. Avila *et al.*, *Chem. Mater.* **31**, 3900 (2019).
- <sup>27</sup>J. M. Woodward *et al.*, *J. Vac. Sci. Technol., A* **40**, 062405 (2022).
- <sup>28</sup>A. Kramida, Yu Ralchenko, J. Reader, and NIST ASD Team, *NIST Atomic Spectra Database (Version 5.8)* (National Institute of Standards and Technology, Gaithersburg, MD, 2020). See <https://physics.nist.gov/asd> (08 September 2021).
- <sup>29</sup>T. Czerwiec, F. Greer, and D. B. Graves, *J. Phys. D: Appl. Phys.* **38**, 4278 (2005).
- <sup>30</sup>D. R. Boris *et al.*, *J. Vac. Sci. Technol., B* **40**, 044002 (2022).
- <sup>31</sup>V. A. Godyak and B. M. Alexandrovich, *Rev. Sci. Instrum.* **88**, 083512 (2017).
- <sup>32</sup>H. C. M. Knoop *et al.*, *J. Vac. Sci. Technol., A* **39**, 062403 (2021).
- <sup>33</sup>M. Zeuner, H. Neumann, and J. Meichsner, *Jpn. J. Appl. Phys.* **36**, 4711 (1997).
- <sup>34</sup>M. Zeuner and J. Meichsner, *Vacuum* **46**, 151 (1995).